Electronic Supporting information for:

Dynamic nuclear polarization NMR of nanosized zirconium phosphate polymer fillers

Fabio Ziarelli,[a] Mario Casciola,[b] Monica Pica,[b] Anna Donnadio,[b] Fabien Aussenac,[c] Claire Sauvée,[d] Donatella Capitani,*[,e] and Stéphane Viel*[,d]

[a]Aix Marseille Université, Centrale Marseille, CNRS, Fédération des Sciences Chimiques FR 1739, 13397, Marseille, France
[b]Università degli studi di Perugia, Dipartimento di Chimica – CEMIN, 06123 Perugia, Italy
[c]Bruker Biospin SAS, 67160 Wissembourg, France
[d]Aix Marseille Université, CNRS, ICR UMR 7273, 13397, Marseille, France
[e]Laboratorio NMR "Annalaura Segre", Istituto di Metodologie Chimiche, CNR, 00015 Monterotondo (Roma), Italy

Outline:

This SI contains a detailed description of experimental protocols, methods and parameters.

1. Chemicals and samples

a. Synthesis of ZrP samples

Functionalized ZrP nanoparticles were prepared as previously reported[1] by reacting a gel of α-type monohydrogen zirconium phosphate nanoparticles[2] with 1,2-epoxydodecane ($C_{12}H_{24}O$) in tetrahydrofuran (Scheme S1A).

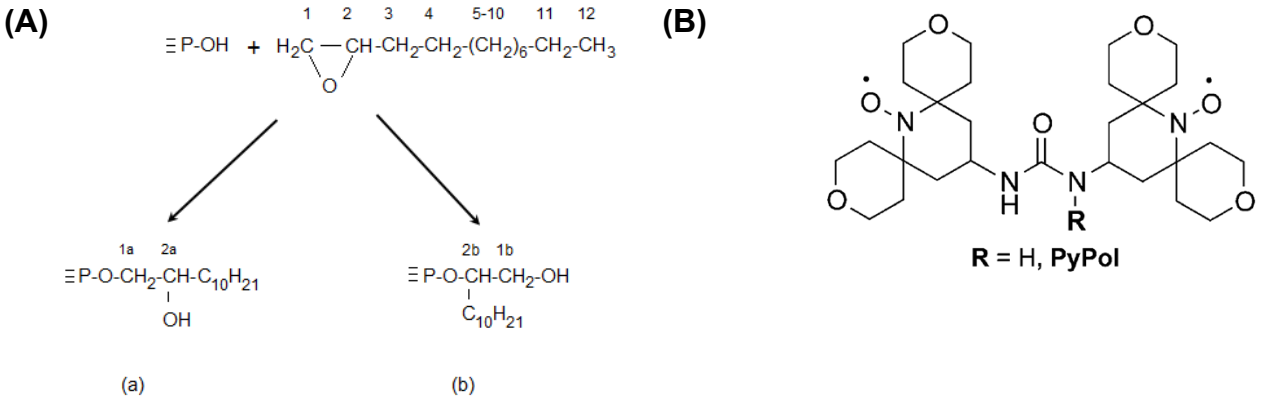

Scheme S1. (A) Expected products for the reaction in THF between 1,2-epoxydodecane and the POH groups of the layers of ZrP nanoparticles. (B) Molecular structure of the PyPOL biradical.

b. Sample preparation for DNP experiments

The DNP polarizing radical used in this study was a dinitroxide known as PyPol (Scheme S1B).[3] This polarizing agent exhibits good water solubility. The sample for DNP SSNMR was prepared by wetting 24.7 mg of grafted ZrP powder in a watch glass with 40 µL of a 14 mM aqueous solution of PyPol. The sample was then stirred with a glass rod to homogeneously wet the solid. During stirring, a slow but continuous loss of sample weight occurred as water evaporated. The resulting partially wet solid (28.8 mg) was eventually transferred into a 3.2 mm (o. d.) MAS sapphire rotor containing a Teflon insert and capped with a zirconium drive cap. The water loss observed during sample preparation was taken into account to estimate the actual weight of the ZrP sample in the rotor (*ca* 20 mg). Note that this sample preparation was repeated three times on three distinct batches of samples, and comparable data were achieved in each case. No other type of preparation methods was tried.

One of the main reasons for using water as a solvent was the total absence of solvent signals in the ^{13}C CPMAS spectrum, as opposed for instance to tetrachloroethane (TCE). TCE is a good DNP solvent but it unfortunately displays a strong ^{13}C resonance in the spectral region of interest (*ca* 75 ppm). Moreover, considering that this study primarily aimed at investigating the surface of the ZrP layers of the nanoparticles, water was appropriate because of its high affinity towards the (predominantly) polar surface of the grafted ZrP nanoparticles. Indeed, although the coupling reaction with 1,2-epoxydodecane is expected to make the surface of the ZrP layers more hydrophobic, the total amount of grafted alkyl chains still remained relatively low with respect to the whole material (and hence to the density of POH groups at the surface of the ZrP layers). Overall, this implied using a hydrophilic DNP polarizing agent (*i.e.* PyPol) as opposed to hydrophobic ones (*e.g.* bCTbK[4] or TEKPol[5]). DNP experiments were also performed using a DMSO/H_2O mixture (67/33, v/v), which is known to form a better glass than pure water at cryogenic temperatures (hereby improving the DNP efficiency). However, in our case, this did not enhance the DNP amplification factor with respect to the use of water only. Moreover, presence of a ^{13}C resonance due to DMSO near 40 ppm in the ^{13}C spectrum was detrimental to the data interpretation.

Finally, ^{1}H DNP build-up time constants were measured on the sample doped with PyPol biradicals (Figure S1). As can be seen, these data could not be properly fitted with a single exponential function but required two exponential functions. Alternatively, a stretched exponential function could also have been used.[6] As previously evidenced in the literature,[7] observation of biphasic build-up time constants suggests that the biradicals are not homogeneously dispersed in the sample, leading to radical-rich and radical-poor regions, which are characterized by relatively low and large build-up time constants, respectively.

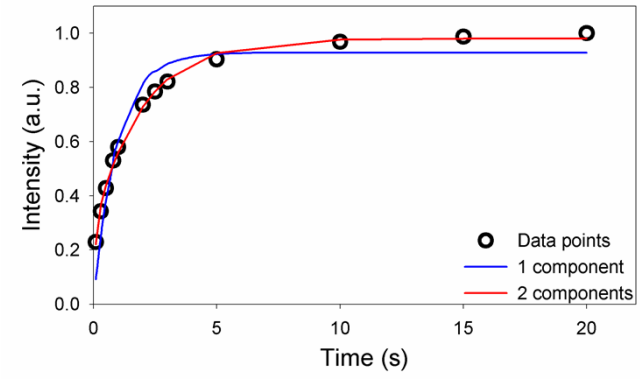

Figure S1. ^{1}H DNP signal build-ups recorded on the ZrP sample doped with PyPol (with the microwave field *on*).

2. NMR experiments

a. NMR hardware and acquisition parameters

All NMR experiments described in this work were recorded on two distinct commercially available Bruker AVANCE spectrometers operating at 9.4 T (400 MHz for the ^{1}H Larmor frequency) and used to record SSNMR and DNP SSNMR experiments, respectively. The former (located at the CNR, Rome, Italy) was controlled by an AVANCE-II console and equipped with a ^{1}H/X 4 mm Magic Angle Spinning (MAS) probe manufactured by Bruker. The latter (located at Bruker Biospin, Wissembourg, France) was controlled by an AVANCE-III console and equipped with a 3.2 mm low-temperature DNP ^{1}H/X/Y MAS probe manufactured by Bruker. The sample temperature was roughly 300 K and 105 K for the SSNMR and DNP SSNMR spectrometers, respectively. The DNP SSNMR spectrometer was equipped with a gyrotron that provided microwave (MW) irradiation of the sample. Specifically, the field sweep coil of the NMR magnet was set so that MW irradiation occurred at the maximum DNP enhancement of TOTAPOL (263.334 GHz).[8] The estimated power of the MW beam at the output of the probe waveguide was ~4 W. The pulse sequence used for CPMAS experiment was as described in the work by Lesage *et al.*,[9] with the MW irradiation field that was either turned *off* or continuously *on*. During Cross Polarization (CP), the amplitude of the ^{1}H contact pulse was linearly ramped in order to improve CP efficiency.[10] Hartmann–Hahn matching conditions and CP contact times were optimized directly on the samples under study. Detailed experimental parameters for all DNP SSNMR and SSNMR experiments can be found in Tables S1 and S2, respectively. Zirconia and sapphire rotors were used for SSNMR and DNP SSNMR, respectively. The rotor used for DNP was sealed with a Teflon insert, while Kel-F and zirconia caps were used for SSNMR or DNP SSNMR rotors, respectively.

Table S1. Parameters used for DNP SSNMR experiments.

Parameters	Experiment		
	^{13}C CPMAS	**^{31}P CPMAS**	**^{31}P–^{13}C HETCOR**
Number of scans	32	16	2048
Recycle delay (s)	3.38 (*)	3.38 (*)	3.0 (*)
Sample spinning rate (Hz)	7000	7000	7000
Sweep width (ppm)	295.8	70	[^{13}C] 295.8; [^{31}P] 60
Acquisition length (ms)	34.4	45.1	34.4
^{1}H 90° pulse (μs)	2.8	2.8	2.8
^{1}H SPINAL-64 decoupling pulse length (μs)	5.6	5.6	5.8
Δt_1 (μs)	-	-	103
Number of increments	-	-	32
Cross-polarization: ^{1}H ➔ ^{13}C			
CP contact time (ms)	1.0	-	-
^{1}H RF field (kHz)	50 (Ramp: 50%-> 100%)	-	-
^{13}C RF field (kHz)	50	-	-
Cross-polarization: ^{1}H ➔ ^{31}P			
CP contact time (ms)	-	2.0	2.0
^{1}H RF field (kHz)	-	50 (Ramp: 50%-> 100%)	50 (Ramp: 50%-> 100%)
^{31}P RF field (kHz)	-	63	63
Cross-polarization: ^{31}P ➔ ^{13}C			
CP contact time (ms)	-	-	4.0 (**)
^{31}P RF field (kHz)	-	-	47 (Ramp: 70%-> 100%)
^{13}C RF field (kHz)	-	-	32

(*) The recycle delay equals 1.3 T_1(^{1}H) except for the 2D experiment. (**) These parameters were optimized to achieve highest sensitivity (see Section 2b).

Table S2. Parameters used for the SSNMR HETCOR experiment.

Parameters	Experiment
	^{1}H–^{13}C HETCOR
Number of scans	320
Recycle delay (s)	2
Sample spinning rate (Hz)	9794
Sweep width (ppm)	[^{13}C] 251.0; [^{31}H] 25.5
Acquisition length (ms)	24.9
90° pulse (μs)	[^{1}H] 3.3
^{1}H FSLG decoupling pulse length (μs)	10.21
^{1}H TPPM-15 decoupling pulse length (μs)	6.6
Δt_1 (μs)	94.24
Number of increments	32
^{1}H➔^{13}C CP contact time (ms)	0.2
^{1}H RF field (kHz)	75
^{13}C RF field (kHz)	50

b. Experimental details regarding data shown in Figure 2

The NMR pulse sequence used to record the experiment reported in Figure 2 is shown in Figure S2.

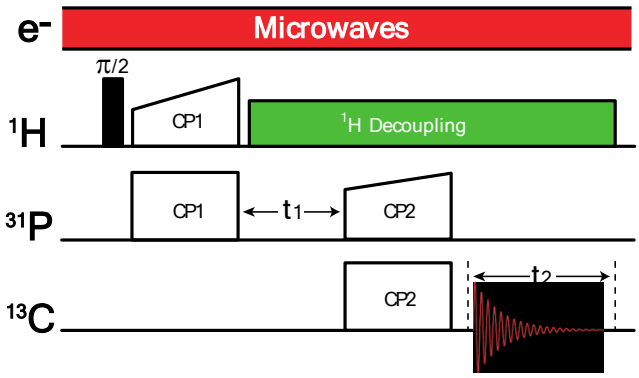

Figure S2. Pulse sequence used to record the two-dimensional ^{31}P–^{13}C DNP SSNMR dipolar correlation experiment reported in Figure 2 in the manuscript.

Key to the success of such experiment is optimization of the second cross polarization transfer (CP2) involving the phosphorous and carbon nuclei. This typically requires precise control over several experimental parameters, including the cross polarization RF field and duration, which are best adjusted by recording a series of experiments on the sample under study (as failure to do so may compromise the experiment success). Thus, this necessary optimization can be prohibitive when sensitivity is an issue. In other words, the impact of the sensitivity gain brought about by DNP is double. Not only can DNP reduce the total duration of the SSNMR experiment itself (by a factor of 100 with respect to comparable SSNMR instrumentation without DNP and at room temperature, see manuscript), but it also allows us to set up the experimental parameters properly by adjusting them directly on the sample under investigation, hereby improving sensitivity *per se* (see Figure S3 for details).

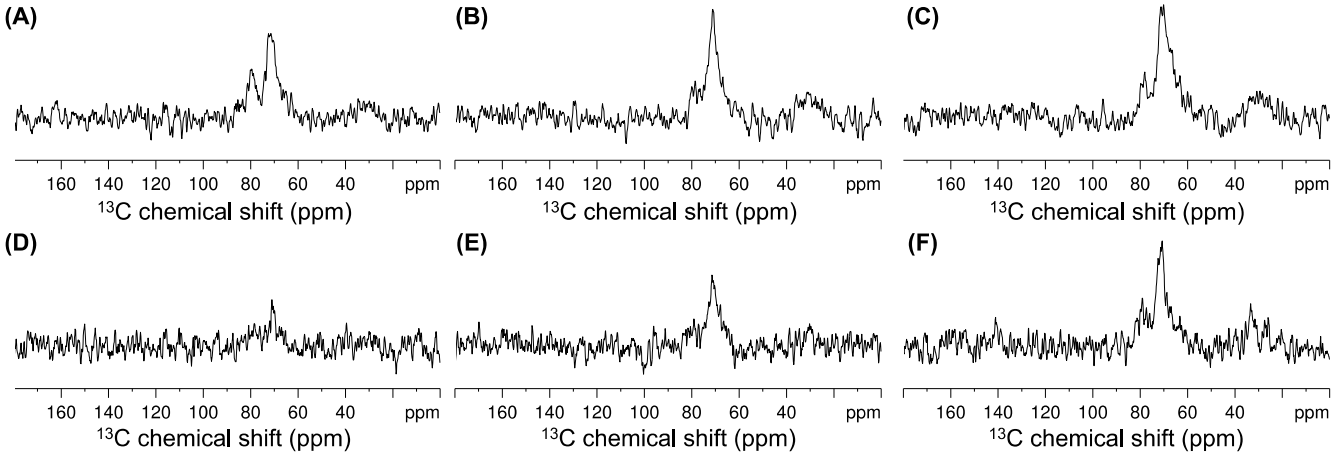

Figure S3. Optimizing CP2 by varying the ^{31}P RF field (A–C) and the contact time (D–F). The ^{31}P RF field values were 44 kHz, 42 kHz and 47 kHz (spectra A, B, and C, respectively, with a 4 ms contact time) whereas the contact times were 1 ms, 2 ms and 6 ms (spectra D, E, and F, respectively, for a 44 kHz ^{31}P RF field). Every experiment took 2h30, for a total duration of 15h (an overnight run). The same optimization without DNP would have required more than 60 days on comparable SSNMR instrumentation without DNP and at room temperature. All of these spectra allowed us to set the ^{31}P RF field to 47 kHz and the contact time to 4 ms.

For the sake of completeness, we also report below (Figure S4) the 1D ^{13}C and ^{31}P projections calculated from the DNP-enhanced 2D ^{31}P-^{13}C spectrum reported in Figure 2 in the manuscript. These projections are compared with the respective DNP-enhanced 1D ^{13}C and ^{31}P CPMAS spectra.

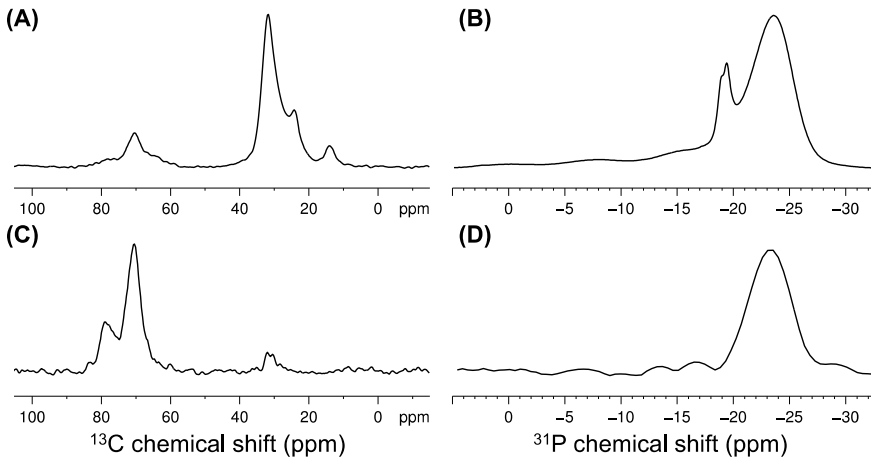

Figure S4. Comparing the (A) ^{13}C and (B) ^{31}P CPMAS spectra with the corresponding 1D ^{13}C and ^{31}P projections (C and D, respectively) calculated from the 2D ^{31}P-^{13}C spectrum reported in Figure 2 in the manuscript.

3. Spectral deconvolution

a. ^{31}P DNP SSNMR CPMAS spectrum

The ^{31}P DNP SSNMR CPMAS spectrum reported in Figure 1A (see manuscript) was deconvoluted using the fitting program introduced by Massiot and co-workers.[11] Results are reported in Figure S5. In addition to the two main forms detected at –23 and –24 ppm (discussed in the manuscript), a few other minor resonances could be observed at about 0, –7, –15 and –19 ppm. Signal at 0 ppm is due to a negligible fraction of free, adsorbed phosphoric acid (H_3PO_4). The resonance at –19 ppm is characteristic of monohydrogen phosphate groups bonded to 3 Zr(IV) atoms in the α-layer, whereas signals at –7 and –15 ppm are due to H_2PO_4 groups bonded to Zr(IV) through two and one oxygen atoms, respectively.[2,12] Finally, analysis of the integrals reported in the Table of Figure S5 shows that the ratio between Form a and Form b was equaled to 2.45 (although this estimation should only be regarded as semi-quantitative because CPMAS data are intrinsically not genuinely quantitative).

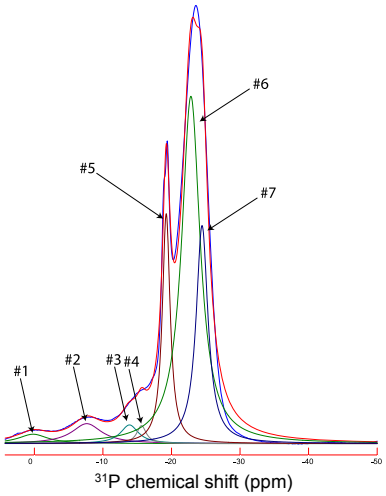

Deconvolution results				
#	δ (ppm)	A (a.u.)	$\Delta\nu_{½}$ (ppm)	I (%)
1	0.2	0.54	5.17	1.9
2	-7.6	1.14	5.25	4.7
3	-13.9	1.07	3.14	2.7
4	-15.6	1.03	1.68	1.4
5	-19.2	13.15	1.37	15.1
6	-22.8	19.86	3.23	52.7
7	-24.4	12.47	2.06	21.5

Figure S5. Deconvolution of the ^{31}P DNP SSNMR CPMAS spectrum reported in Figure 1A.

b. *^{13}C DNP SSNMR CPMAS spectrum*

The ^{13}C DNP SSNMR CPMAS spectrum (Figure 1B in the manuscript) was also deconvoluted by using the same fitting program in order to confirm the assignment of the 50-100 ppm spectral region derived from this work (see Figure S6).

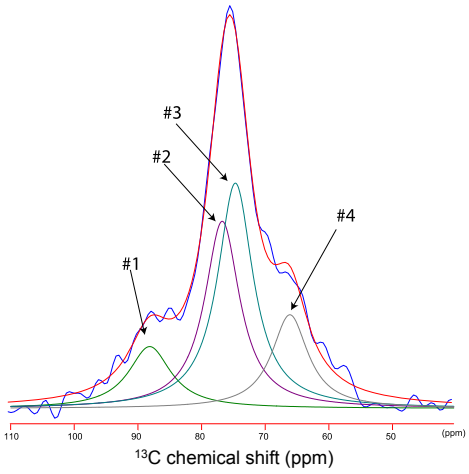

Deconvolution results					
#	□□□□□□ □□□□ (*)	δ (ppm)	A (a.u.)	$\Delta\nu_{½}$ (ppm)	I (%)
1	2b	78.5	0.17	5.08	12.5
2	1a (**)	71.3	0.50	4.20	32.0
3	2a (**)	70.0	0.60	4.25	39.0
4	1b	64.6	0.25	4.35	16.5

(*) See Figure 2 in the manuscript for atom labeling. (**) These assignments could be interchanged.

Figure S6. Deconvolution of the ^{13}C DNP SSNMR CPMAS spectrum reported in Figure 1B.

Results reported in Figure S6 shows that the spectral lineshape in this specific region can be properly reproduced by using a total of 4 Gaussian resonances at about 79 ppm, 71 ppm, 70 ppm, and 65 ppm. More importantly, the ratio between the combined integrals of signals #2 and #3 (assigned to carbons 1a and 2a) to the combined integrals of signals #1 and #4 (assigned to carbons 2b and 1b, respectively) is found to be 2.47. This is in excellent agreement with the Form a / Form b ratio derived from the analysis of the ^{31}P CPMAS spectrum in Section 3b (a ratio of 2.45 was obtained). Again, because these data originated from a CPMAS spectrum, they should only be considered as semi-quantitative.

4. References

1. M. Casciola, D. Capitani, A. Donnadio, G. Munari and M. Pica, *Inorg. Chem.*, 2010, **49**, 3329-3336.
2. M. Pica, A. Donnadio, D. Capitani, R. Vivani, E. Troni and M. Casciola, *Inorg. Chem.*, 2011, **50**, 11623-11630.
3. C. Sauvée, M. Rosay, G. Casano, F. Aussenac, R. T. Weber, O. Ouari and P. Tordo, *Angew. Chem.-Int. Ed.*, 2013, **52**, 10858-10861.
4. A. Zagdoun, G. Casano, O. Ouari, G. Lapadula, A. J. Rossini, M. Lelli, M. Baffert, D. Gajan, L. Veyre, W. E. Maas, M. Rosay, R. T. Weber, C. Thieuleux, C. Coperet, A. Lesage, P. Tordo and L. Emsley, *J. Am. Chem. Soc.*, 2012, **134**, 2284-2291.
5. A. Zagdoun, G. Casano, O. Ouari, M. Schwarzwälder, A. J. Rossini, F. Aussenac, M. Yulikov, G. Jeschke, C. Copéret, A. Lesage, P. Tordo and L. Emsley, *J. Am. Chem. Soc.*, 2013, **135**, 12790-12797.
6. A. J. Rossini, A. Zagdoun, F. Hegner, M. Schwarzwalder, D. Gajan, C. Coperet, A. Lesage and L. Emsley, *J. Am. Chem. Soc.*, 2012, **134**, 16899-16908.
7. T. C. Ong, M. L. Mak-Jurkauskas, J. J. Walish, V. K. Michaelis, B. Corzilius, A. A. Smith, A. M. Clausen, J. C. Cheetham, T. M. Swager and R. G. Griffin, *J. Phys. Chem. B*, 2013, **117**, 3040-3046.
8. C. S. Song, K. N. Hu, C. G. Joo, T. M. Swager and R. G. Griffin, *J. Am. Chem. Soc.*, 2006, **128**, 11385-11390.
9. A. Lesage, M. Lelli, D. Gajan, M. A. Caporini, V. Vitzthum, P. Mieville, J. Alauzun, A. Roussey, C. Thieuleux, A. Mehdi, G. Bodenhausen, C. Coperet and L. Emsley, *J. Am. Chem. Soc.*, 2010, **132**, 15459-15461.
10. G. Metz, X. Wu and S. O. Smith, *J. Magn. Reson. Ser. A*, 1994, **110**, 219-227.
11. D. Massiot, F. Fayon, M. Capron, I. King, S. Le Calvé, B. Alonso, J.-O. Durand, B. Bujoli, Z. Gan and G. Hoatson, *Magn. Reson. Chem.*, 2002, **40**, 70-76.
12. M. Pica, A. Donnadio, E. Troni, D. Capitani and M. Casciola, *Inorg. Chem.*, 2013, **52**, 7680-7687.